Composites Science and Technology 135 (2016) 83–91

Contents lists available at ScienceDirect

Composites Science and Technology

journal homepage: http://www.elsevier.com/locate/compscitech

Synergistic effect of BN and graphene nanosheets in 3D framework on the enhancement of thermal conductive properties of polymeric composites

Linbo Shao [a, b], Liyi Shi [b, **], Xuheng Li [a], Na Song [a], Peng Ding [a, *]

[a] Research Center of Nanoscience and Nanotechnology, Shanghai University, 99 Shangda Road, Shanghai 200444, PR China
[b] College of Sciences, Shanghai University, 99 Shangda Road, Shanghai 200444, PR China

ARTICLE INFO

Article history:
Received 10 August 2016
Received in revised form
14 September 2016
Accepted 16 September 2016
Available online 17 September 2016

Keywords:
Thermal conductive polymer composites
Boron nitride
Graphene
3D framework
Synergistic effect

ABSTRACT

In this work, we reported a synergistic effect of boron nitride nanosheets (BNNSs) with graphene in the 3D BNNSs/graphene framework (BGF) on the enhancement of thermal conductive properties of polyamide-6 (PA6) composites. The 3D BGF was self-assembled by embedding BNNSs into 3D graphene framework (GF). And the PA6 composites were obtained by in-situ polymerization of PA6 chains in the pores of the 3D framework. The thermal conductivity (TC) of PA6 composites with BGF (1.6 wt% BNNS/6.8 wt% graphene) was improved to 0.891 $W \cdot m^{-1} \cdot K^{-1}$. This value indicated that additional introduction of 1.6 wt% BNNSs could increase the TC up to 87.6% and 350% compared with the composites containing 6.8 wt% 3D GF (0.475 $W \cdot m^{-1} \cdot K^{-1}$) and neat PA6 (0.196 $W \cdot m^{-1} \cdot K^{-1}$), respectively. The high efficiency of BNNSs on the TC enhancement could be attributed to the factors including the unobstructed 3D thermal conductive paths constructed by BNNSs, and the morphology-promoted synergistic effect between BNNSs and graphene nanosheets.

1. Introduction

Thermal conductive polymeric composites have attracted much attention because of their broad applications in electronic, high-temperature dielectric and energy storage devices [1,2]. Quite a few of methods were carried out to obtain the composites with high thermal conductive properties [3]. Careful revision can be found that the most fundamental strategy embodied in these methods is to construct unobstructed thermal conductive paths in the polymer matrix. For example, a common method to enhance a polymer's thermal conductivity (TC) is to blend it with high-TC fillers such as metal or ceramic particles [4]. With the increasing of the amount of filler, the thermal conductivity of composites increased slowly until the filler fraction reached a percolation threshold where a rapid increase in conductivity started. Fillers had to form a random close-packed structure to maximize a pathway or network for heat conduction through the polymer matrix. However, the large amount of fillers required to exceed the percolation threshold can not only deteriorate the superior performance of polymer matrix such as electrical and optical properties, but may also significantly increase the material cost [5]. Therefore, it is a challenge and a hot topic to improve their thermal conductive efficiency or reduce the amount of fillers [6].

Layered inorganic nanomaterials, such as graphene and BNNSs, were proved to be a good choice to set up a thermal conductive path due to their high TC and large aspect ratio [7–9]. For example, Yu et al. [10] regulated aspect ratio of the graphite nanoplatelets (GNP, ~5 vol%) from 3 to 200 and finally obtained the epoxy nanocomposites with the TC up to 1.45 $W \cdot m^{-1} \cdot K^{-1}$. A recent work by Ganguli et al. [11] revealed that a 55% (0.30 $W \cdot m^{-1} \cdot K^{-1}$) increase of TC had been reached in the composite with a 2 wt% silane-treated GNPs dispersed in epoxy matrix. While the TC further enhanced by 28-fold (5.8 $W \cdot m^{-1} \cdot K^{-1}$) when the GNPs loading was up to 20 wt%. In this case, the aforementioned problems still exist, especially that when the filler content is high, it is very difficult to uniformly disperse these layered fillers in polymer composites [12,13]. Though the filler's aggregation could be avoided to a certain degree by surface modification, the excessive modification would destroy the lamellar structure and thus reduce the effects of the fillers on TC enhancement [14–17]. So recently, the combined use of hybrid fillers was proposed as one solution for improve the thermal

* Corresponding author.
** Corresponding author.
E-mail addresses: shiliyi@shu.edu.cn (L. Shi), dingpeng@shu.edu.cn (P. Ding).

http://dx.doi.org/10.1016/j.compscitech.2016.09.013
0266-3538/

conductive efficiency in polymer composites [18–21]. Yu et al. [22] reported that the TC of the grease composites containing 63 vol % alumina was 2.7 $W \cdot m^{-1} \cdot K^{-1}$; and the TC enhanced by 28% (to 3.45 $W \cdot m^{-1} \cdot K^{-1}$) after further compounded with 1 wt% graphene. Another work by Tsai et al. [23] blended functionalized BN and glycidy-methacrylate-grafted graphene with polyimide (PI) to fabricate a thermal conductive PI composites. TC increased from 0.13 $W \cdot m^{-1} \cdot K^{-1}$ of neat PI to 2.21 $W \cdot m^{-1} \cdot K^{-1}$ of thermal conductive PI composites. Our group also studied the effect of the BN and graphene hybrid fillers on the TC improvement in polymeric composites and proposed a morphology-promoted synergistic effect between graphene and BN nanolayers [18].

In the present work, we further demonstrated a synergistic effect of BN nanosheets (BNNSs) with graphene in a 3D framework on the enhancement of thermal conductive of PA6 composites. The 3D BN/graphene framework (BGF) was obtained by assemble BNNSs and graphene oxide (GO) with the hydrothermal reduction and freeze-drying process. PA6/BGF (PBGF) composites were prepared by the in-situ "grafting to" strategy, in which the PA6 chains were covalently grafted on the 3D framework. The TC of PA6 composites with BGF (1.6 wt% BNNS/6.8 wt% graphene) was improved to 0.891 $W \cdot m^{-1} \cdot K^{-1}$. This value indicated that additional introduction of 1.6 wt% BNNSs could increase the TC up to 87.6% and 350% compared with the composites containing 6.8 wt% 3D graphene (0.475 $W \cdot m^{-1} \cdot K^{-1}$) and neat PA6 (0.196 $W \cdot m^{-1} \cdot K^{-1}$), respectively. As far as we know, the synergistic effect of BNNSs and graphene in a hybrid 3D framework has not been observed previously. The obtained polymeric materials could be applied in thermal interface materials, polymer dielectrics, and other high-performance thermal management system [1].

2. Experimental section

2.1. Materials

Natural graphite flakes were purchased from Qingdao Jinrilai Co., Ltd. (Qingdao, China). Concentrated sulfuric acid (98.0% H_2SO_4), potassium permanganate ($KMnO_4$), hydrogen peroxide (30% H_2O_2), hydrochloric acid (HCl), formic acid (85% HCOOH) were obtained from Sinopharm Chemical Reagent Co., Ltd. h-BN power (1 μm), Dimethyl formamide (DMF, 99%), ε-caprolactam and 6-aminocaproic acid were all purchased from Sigma-Aldrich Co., Ltd. All the agents were used as received without further treatment.

2.2. Preparation of GO and BNNSs

The preparation process of BNNSs, BGFs and PBGFs composites was shown in Fig. 1. First, BNNSs were prepared by solution exfoliation of the BN powder with a tip-type sonication process which is a widely-used method [24,25]. In a typical procedure, 1 g h-BN powder was dispersed in 40 mL DMF, and then vigorously sonicated for 10 h using a tip-type sonication machine (Bilon 1000Y, Shanghai Bilon Instrument Manufacturing Co., Ltd). After sonication, the solution was centrifuged for 30 min at 1500 rpm by a fractional centrifugation (TGL-10C, Shanghai Anting Scientific Instrument Factory, China). The BNNSs peeled away from h-BN powder were

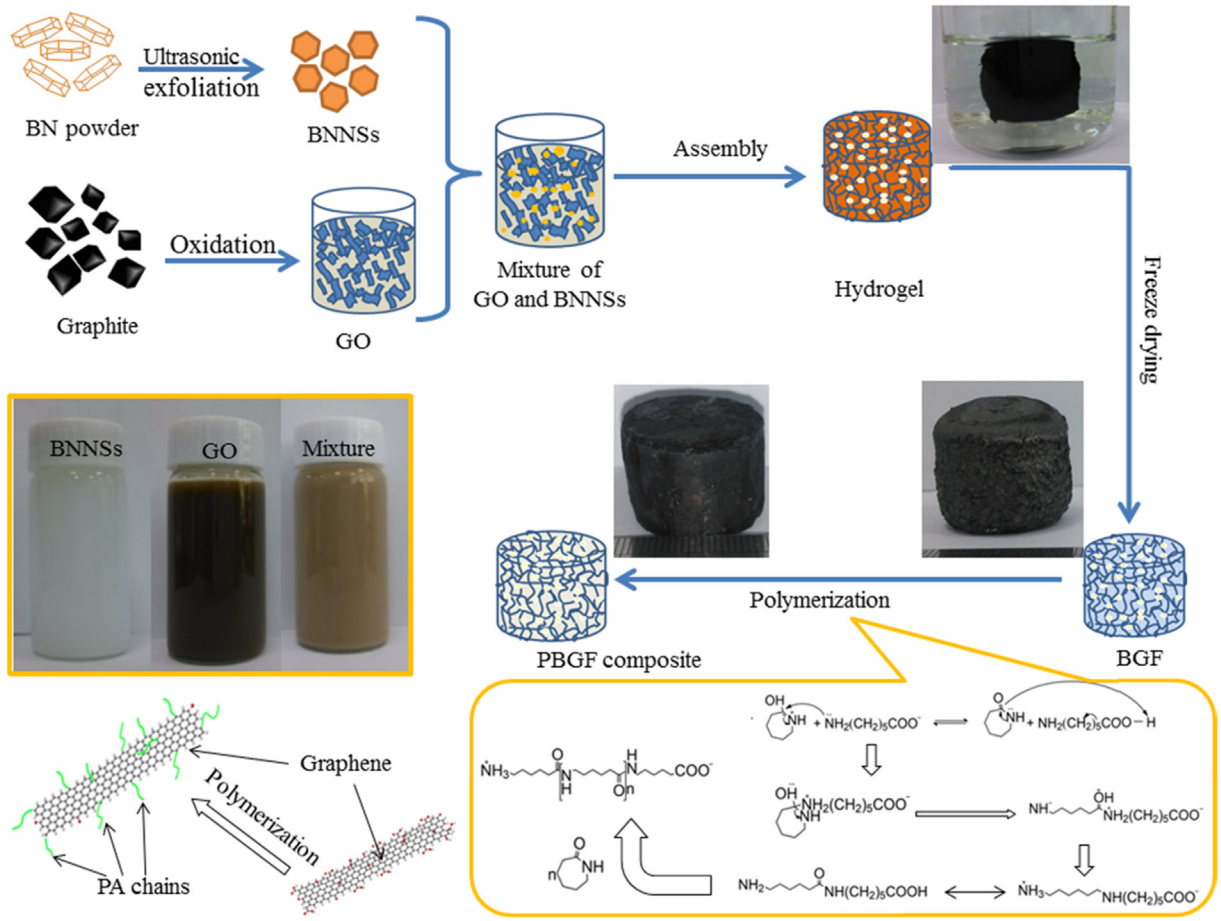

Fig. 1. Schematic of the synthesis procedure of PBGF composites. Images of BNNSs and GO solutions, BNNSs/graphene hydrogel, BGF and PBGF composites.

dispersed in whitish supernatant (~0.22 mg/mL). The resultant whitish supernatant was centrifuged for another 30 min at 10000 rpm. Finally, one unit of BNNSs of approximately 8.8 mg was obtained after removing the transparent supernatant solvent. GO was prepared from graphite powder using the pressurized oxidation method reported elsewhere [26]. In a typical procedure, graphite powder (5 g), $KMnO_4$ (25 g) and concentrated sulfuric acid (250 mL) were sealed in a Teflon autoclave (500 mL) and completely cooled down at 0–4 °C. Then reacted at 80 °C for 1.5 h, the obtained mud was poured in deionized water (1000 mL). After the solution cooled to room temperature, H_2O_2 solution was dropwise added into the solution (until no bubbles form) to neutralize residual oxidizing agents. The obtained GO was acid-washed for several times.

2.3. Preparation of BGF

BGF was prepared by self-assembly of BNNSs and GO layers in the hydro-thermal reduction process. 40 mL GO suspension (10 mg/mL) was mixed with a designed amount of BNNSs and then sonicated for 2 h to make BNNSs and GO well dispersed and mixed in the solution. The mixture was sealed in a 100 mL Teflon autoclave and maintained at 160 °C for 7 h. After the self-assembly and reduction process, a cylinder-shaped hydrogel could be obtained. The hydrogel was immersed in deionized water for 48 h to remove the acid generated in the reduction process. And then the hydrogel was freeze-dried at −60 °C for 48 h to form a black porous BGF. BGFs contain 2, 4, 6, 8 unites of BNNSs were noted as B2GF, B4GF, B6GF and B8GF.

2.4. Preparation of PBGF composites

ε-caprolactam (36 g), 6-aminocaproic acid (4 g) and BGF were put into a three-neck round-bottom flask (100 mL). Under nitrogen flow, the mixture was heated to 100 °C for 30 min for the pre-polymerization and simultaneously removing the adsorbed water. Then the mixture was further heated to 180 °C under vacuum. At this stage, BGF was infiltrated and submerged into the melted polymer precursor. The mixture was maintained 180 °C for 1 h, and then heated to 250 °C for 5 h. After cooling to room temperature, the resultant PBGF composites block was washed in boiling deionized water for 2 h to remove the monomer and the oligomers with low molecular weight. The washed PBGF composites sample was dried at 80 °C for 10 h. Finally, the cylinder-shaped PBGF composites samples were mechanically cut out from the block. For comparison, the PA6/crushed-BGF composites were prepared by manually crushing BGF composites. The crushed-BGF and ε-caprolactam (9.0 g), 6-aminocaproic acid (1.0 g) were used to synthesis PA6/crushed-BGF composites in the same process as the PBGF composites.

2.5. Characterization

The morphologies and microstructures of the sample were investigated by Scanning electron microscopy (SEM, JSM-6700F, JEOL, Japan), Transmission electron microscopy (TEM,200CX, JEOL, Japan), Fourier-transform infrared (FTIR, AVATAR 370, Nicolet, USA), X-ray photoelectron spectroscopy (XPS, RBD upgraded PHI-5000CESCA, Perkin Elmer, USA), Raman (INVIA, Renishaw PLC, UK), and X-ray diffraction (XRD, D/max-2200/PC, Rigaku, Japan). Thermal gravimetric analysis (TGA) was performed on a Netzsch STA409PC simultaneous thermal analyzer. The data of TGA was collected from room temperature to 700 °C with the heating rate of 10 °C·min^{-1} under a nitrogen atmosphere. The viscosity measurement of PBGF composites dissolved in 85% formic acid with a concentration of 0.5 g dL^{-1} was carried out in an Ubbelohde viscometer at 25 °C. The TC of PG composites was measured by a Netzsch LFA 447 Nanoflash at 25 °C.

3. Results and discussion

3.1. Preparation and characterization of BGF samples

h-BN can be exfoliated to mono- or few-layer 2D nanosheets via sonication with the help of DMF solvent molecules entering the lattice of the sheets as reported in previous work [18,27]. As shown in Fig. 1, BNNSs and GO could be homogeneously dispersed in water. The mixed solution of BNNSs and GO was light brown and homogeneous in visual observation and maintained the uniform dispersion in several days, which ensured BNNSs uniformly distribute in BGFs. Few-layered BNNSs were clearly identified by the edges of the BN sheets with a lateral size at 200–400 nm as shown in the TEM image (Fig. 2a). The XRD pattern (Fig. 3a) of BNNSs showed a typical curve of a hexagonal crystal, where the diffraction peaks centered at$2\theta = 27°$, $2\theta = 41.6°$ and 55.2° were corresponding to the (002), (100) and (004) reflections of the h-BN respectively. The (002) peak was strong and sharp which suits the characteristic of exfoliated BNNSs [28,29].

GO represented layered structure in TEM image as shown in Fig. 2b. It can be seen that the GO sheets were stacked by 2–5 GO monolayers and the lateral size was about 1–2 μm. Due to the size discrepancies between BNNSs and GO sheets, the GO sheets could be used to load BNNSs in BGFs. The FTIR spectrum of GO (Fig. 3b) showed the absorption peaks of C=C skeletal vibrations and

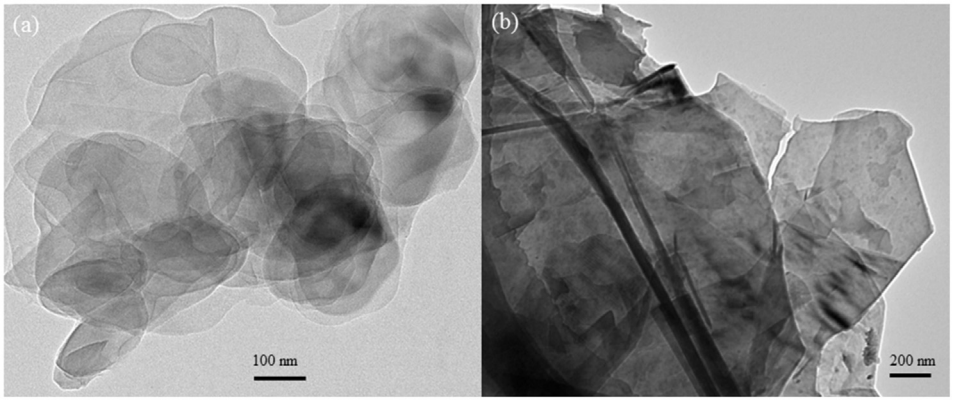

Fig. 2. TEM image of BNNSs (a) and GO (b).

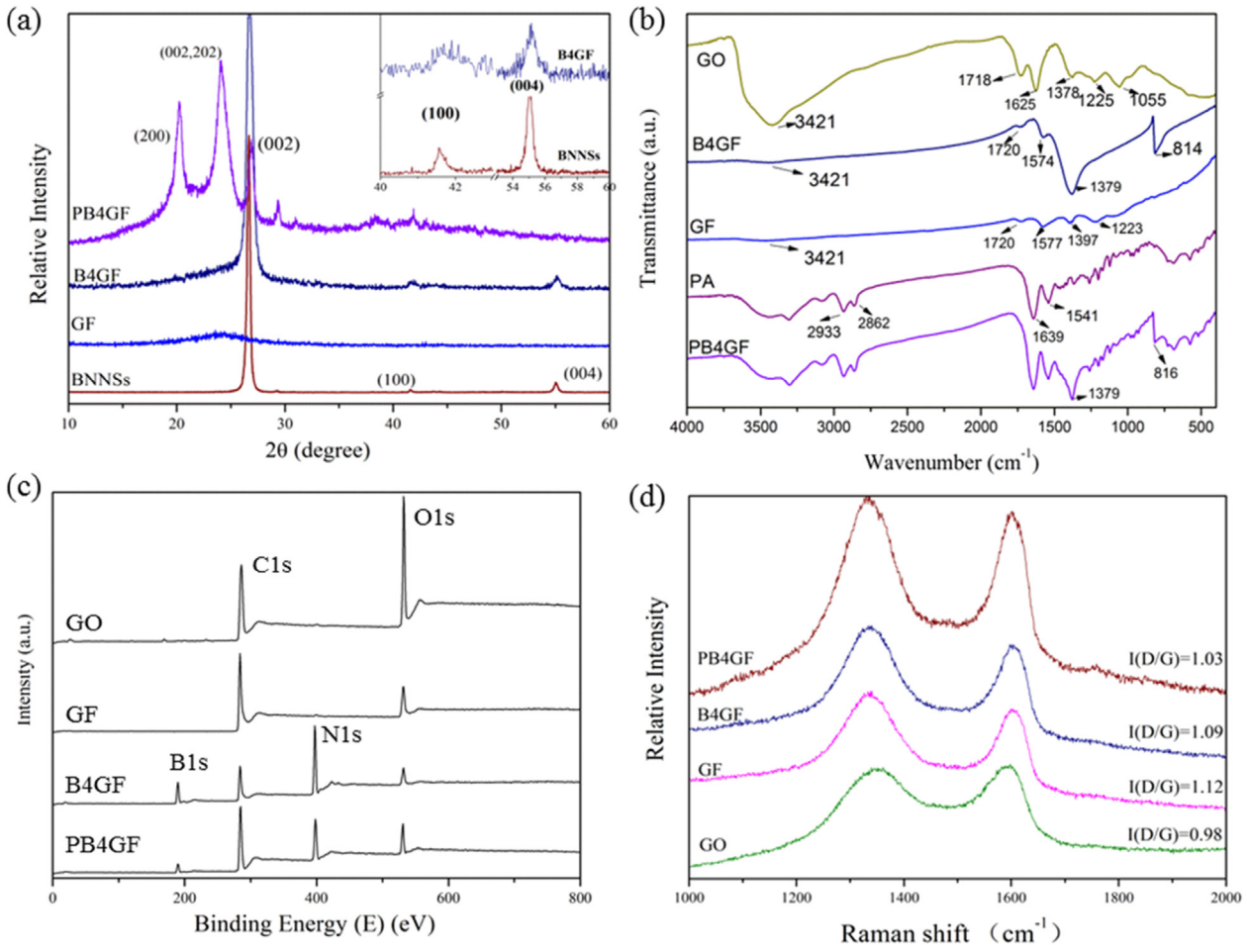

Fig. 3. Characterization of GO, BNNSs, GF, BGF, and PBGF composites. a: XRD patterns with the insets showing the magnification; b: FTIR spectra; c: XPS spectra; d: Raman spectra.

stretching of oxygenous groups such as alkoxy C–O, epoxy C–O, O–H (carboxyl) and C=O [7]. XPS analysis (Fig. 3c) of GO also confirmed the oxidation of GO. The atomic ratio of GO, GF, BGF and PBGF composites calculated according to XPS test was given in Table S1. The C/O atomic ratio of GO was 66.1/34.9. The C1s XPS spectrum of GO (Fig. 4a) was split into four peaks which confirmed the SP^2C– SP^2C (284.7 eV), C–OH (285.7 eV), C–O (287.0 eV) and C=O (288.6 eV) bonds. The above results confirmed the successful oxidization of graphite.

After the hydrothermal reduction, it formed a BNNSs/graphene hydrogel and the turbid solution became clean and transparent (Fig. 1), indicating the BNNSs were captured by the graphene network and embedded into the BGF [30]. After freeze-drying, BGF with light black color and cylindrical shape was obtained. BGFs with different content of BNNSs were noted as B2GF, B4GF, B6GF and B8GF.

GF was obtained without BNNSs addition in the hydrothermal reduction process. The SEM image of GF sample showed that graphene sheets were stacked and connected to form a 3D framework (Fig. 5a). The pore sizes of GF were ranging from tens to over a hundred of micrometers and the pore walls consisted of thin layers of stacked graphene sheets. The pores in GF were interconnected, which allows it to be easily saturated with the reactants and filled with polymer chains after polymerization. SEM image of BGF sample were shown in Fig. 5b and c, BGF remained porous structures even after doped by 8 units of BNNSs. BNNSs were uniformly distributed in BGF and attached to the GF. The XRD patterns (Fig. 3a) GF sample showed a broad peak centered at $2\theta = 24°$, implying that the obtained GF was composed of randomly ordered graphene sheets with a corrugated structure [31]. For BGF sample, the (002) peak of BNNSs at $2\theta = 27°$ was not zygomorphic. It is because that the weak peak of randomly ordered graphene sheets was covered by the strong (002) peak of BNNSs and uplifted the curve at $2\theta = 24°$. The strong diffraction peaks of BNNSs indicated that BNNSs existed in the GF. BGFs containing different amount of BNNSs gave similar XRD curves (Fig. S1). The FTIR spectrum of GF sample (Fig. 3b) showed that the peaks corresponding to the oxygenous groups were decreased compare with GO sample. This indicates that oxygenous groups were partly removed after the hydro-thermal reduction. Moreover, compared with GF, the FTIR spectrum of BGF sample had two new peaks at 816 and 1379 cm^{-1}, which were caused by the B–N–B out-of-plane bending vibration and the in-plane B–N transverse optical modes [29] evidenced the assembly of BNNSs. The XPS spectra of GF were shown in (Fig. 3c). The O_{1s} peak of GF significantly decreased compared with GO samples. The O atomic ratio reduced from 33.9% of GO to 16.4% of GF. On the other hand, the C/O atomic ratio of BGF (81.3/18.7) was similar to GF (83.6/16.4), which indicated GO was reduced in the hydrothermal reduction and the reduction degree of GO sheets in BGF samples was similar to that of GF samples. Moreover, the C_{1s} XPS spectra of GF and BGF (Fig. 4b and c) showed that the peaks of C–O groups (287.0 eV) in GF and BGF were decreased rather than disappeared, indicating the oxygenous groups were partly preserved in the procedure of hydrothermal reduction. These residual

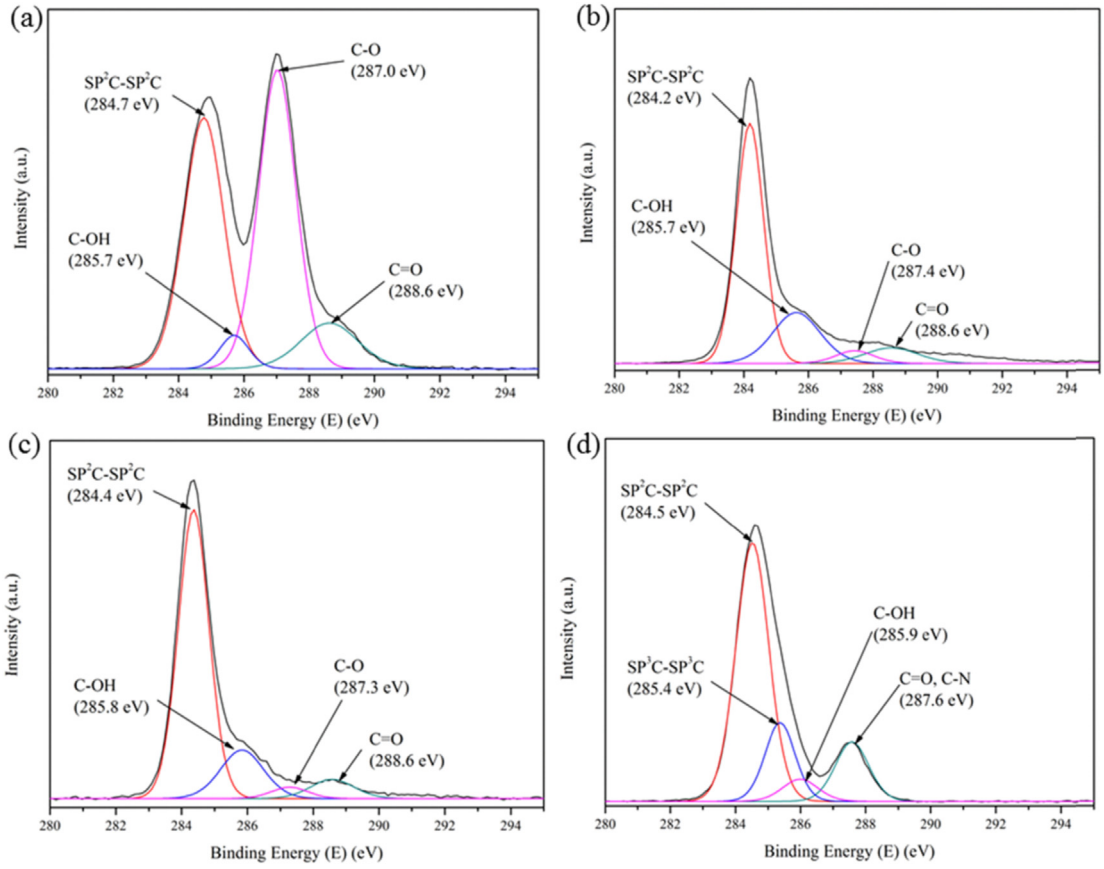

Fig. 4. C1s spectra of GO (a), GF (b), B4GF (c), and PB4GF composites (d).

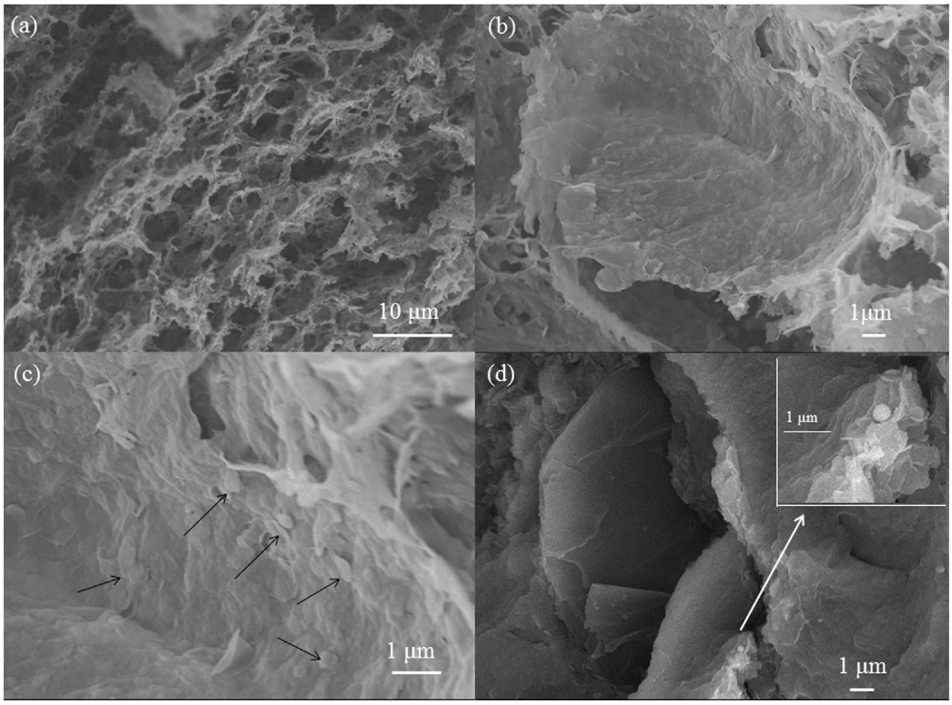

Fig. 5. SEM image of GF(a), BGF(b) and (c) and PBGF composites(d) (The inset show the magnification). The BNNSs in BGF is pointed by the black arrow.

groups were the react points for the following in-situ polymerization of PBGF composites. The O_{1s} XPS spectra (Fig. S2) of GF and BGF also confirmed the preservation of oxygenous groups on the graphene sheets.

The Raman spectrum of GO, GF, BGF and PBGF composites were shown in Fig. 3d. GO represents two typical bands indexed at ~1353 and ~1597 cm^{-1}, which are attributed to the well-documented D and G bands of GO [32]. After the hydrothermal reduction, GF and BGF showed similar peak position of D and G bands with GO, as reported in previous work [33,34]. However, the I (D/G) of GF (1.12) and BGF (1.09) were slightly higher than GO (0.98). This might be due to the defects formed in the high-temperature hydro-thermal reduction.

3.2. Structure and characterization of PBGF composites

The PBGF composites were obtained by the in-situ "grafting to" strategy as reported in our previous work [7,35,36]. As shown in Fig. 1, at high temperature, ε-caprolactam was initiated by 6-aminocaproic acid to conduct the ring-opening polymerization. With the consumption of ε-caprolactam monomers, the PA6 chains gradually propagated. The active PA6 chains moved into the pores of 3D framework, and at the same time, were immobilized onto the GO sheets by the condensation reaction between the active amino groups at PA6-chain terminals and the aforementioned residual carboxyl acid groups on GO sheets. Following the continuous propagation of PA6 chains, the viscosity of the mixture increased synchronously. And the PBGF composites were obtained.

The viscosity-average molecular weight (M_η) of PBGF composites and neat PA 6 was measured by Ubbelohde viscometer (see details in Supporting Information). The M_η of neat PA6 was calculated at about 30.2×10^3 g/mol and the M_η of grafting PA6 chains in PBGF composites slightly decreased to $21.5\pm 2.0\times10^3$ g/mol (Fig. S3). The M_η of PBGF composites was slightly decreased compare with neat PA6, this is due to polymerization of PBGF composites was in limited space. And similar phenomena were also found in previous work [3,7].

The morphology of the PBGF composites was observed by SEM analysis (see Fig. 5d). BGF has been completely infiltrated with PA. The curved graphene sheets attached on PA6 block due to the condensation reaction between the remaining oxygenous groups on graphene and the active amino groups at PA6-chain terminals. The XRD pattern of PBGF composites was given in Fig. 3a. The diffraction peaks at $2\theta = 20^\circ$ and 24° were corresponding to (200) and (002,202) reflections of α-form PA6 crystal. The diffraction peaks at $2\theta = 27^\circ$, 42° and 56° were corresponding to (002), (100) and (004) reflections of BNNSs respectively. The XRD result evidenced that BNNSs remained their crystal structure in the PBGF composites after the polymerization process.

In the FTIR curves of PBGF composites (Fig. 3b), the characteristic peaks of amide (−C(O)NH−) stretching vibration at 1541 and 1639 cm^{-1} indicated the presence of the amide bond formed by the reaction between GO and PA6 chains. Additionally, methylene ($-CH_2-$) stretching vibration at 2933 and 2862 cm^{-1} was also from the pendant PA6 chains [7]. Moreover, compared with neat PA6, the FTIR spectrum of PBGF composites had characteristic peaks of BNNSs centered ~816 and ~1379 cm^{-1}, which confirmed BNNSs were remained in PBGF composites. The XPS spectra (Fig. 3c) of PBGF composites showed that the C1s and N1s peak increased after the polymerization. The C/O/N/B atomic ratio of PBGF composite was 57.2/9.4/20.7/12.7. Compare to B atomic content, the additional N atomic content came from amino groups in PA6. The C1s spectra of PBGF composites (Fig. 4d) were split into four peaks [37]. In contrast to the C1s spectra of BGF (Fig. 4c), the additional peak of SP^3C-SP^3C (285.4 eV), C═O and C−N (287.6eV) bonds in PBGF composites belongs to carbon chains and amide bonds in PA6. The peak of SP^2C-SP^2C (284.5 eV) belongs to graphene, indicated the graphene was preserved in PBGF composites. These above results demonstrated that BNNSs were successfully introduced to BGFs and PBGF composites and BGF was preserved in the PBGF composites.

3.3. Thermal conductivity of PBGF composites

Fig. 6 displayed the TC of PBGF composites with varied BNNSs content by "through plane" method with a Netzsch LFA 447 Nanoflash at 25 °C (see Surpporting Information). The TC increased from 0.196 $W\cdot m^{-1}\cdot K^{-1}$ of neat PA6 to 0.475 $W\cdot m^{-1}\cdot K^{-1}$ of PGF with 6.8 wt% GF loading. This TC improvement originated from the thermal conductive path of 3D GF and favorable grafting between PA6 chains and GF in in-situ polymerization [38,39]. With the increase of BNNSs content, as shown in Fig. 6a, TC of the composites increased consistently. TC of PB8GF composites reached up to 0.891 $W\cdot m^{-1}\cdot K^{-1}$, improved by 87.6% compared to PGF and 350% to neat PA6. It can be found from Table S2 that the BNNSs had more efficient synergistic effect with GF than other inorganic fillers on

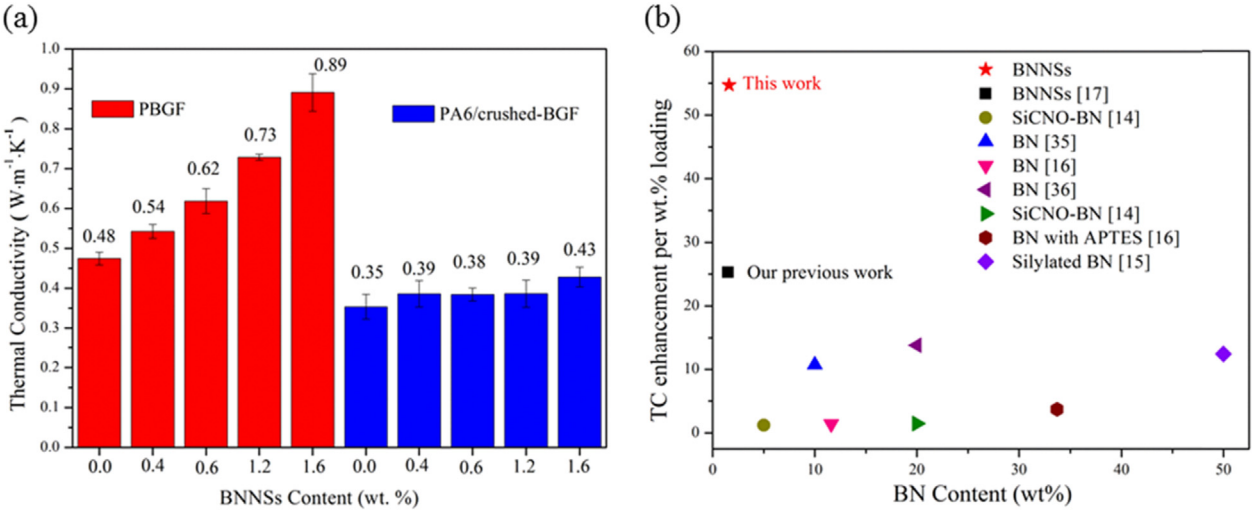

Fig. 6. (a) TC of PBGF composites and PA6/crushed-BGF composites. (b) Comparisons on the TC enhancement efficiency of BNNSs to composites.

the improvement of the TC of polymeric composites. For example, the TC of PA66 composites with 20 wt% SiCNO-BN loading is 0.424 $W \cdot m^{-1} \cdot K^{-1}$ [15]; the TC of PPS composites with 2.0 wt% CNT and 10 wt% BN loading is 0.58 $W \cdot m^{-1} \cdot K^{-1}$ [40]. TC enhancement efficiency of BNNSs to composites is characterized by TC enhancement per 1 wt% loading (η), which is defined as

$$\eta = \frac{TC - TC_0}{100\ W\ TC_0} \times 100\%$$

where, TC and TC_0 are the thermal conductivities of the composites with BNNSs loading and matrix without BNNSs loading, respectively; W is the weight loading of BNNSs in composites. Fig. 6b gave the η as a function of BNNSs loading for polymer composites. One can see that the η in this work is the highest value among the previous researches focused on the thermal conductive composites based on thermoplastic polymer matrixes, to the best of our knowledge. Compared with previous investigations about BN-based polymeric composites, similar TC value often required higher wt% filler content, generally ten times than the present work (Fig. S4) [15–18,40,41].

In the present work, we proposed that the TC of composites were improved due to the synergistic properties between BNNSs and graphene sheets in a hybrid 3D framework and the simulation schematic was shown in Fig. 7. Compare to the traditional using hybrid thermal conductive filler, this hybrid 3D network provided the following advantages. First, the aligned BNNSs provides additional thermal conductive path. As shown schematically in Fig. 7, BNNSs arranged to be a 3D thermal conductive path by using the 3D GF as a template. The arrangement of thermal conductive filler into a multidimensional thermally conductive path was also reported in previous works [21,42–44]. To further prove the significance of preserving 3D framework for the TC, PA6/crushed-BGF composites samples were prepared using crushed BGFs. SEM image of the PA6/crushed-BGF composite (surface eroded by formic acid) was shown in (Fig. 8a). One can see that BGF was broken up into small pieces, the continuous 3D BGF no more existed.

Compare with PBGF composites, the TC of PA6/crushed-BGF composites reduces along with the BNNSs content (see Fig. 6a). The TC of PGF composites reduced 27% from 0.48 $W \cdot m^{-1} \cdot K^{-1}$ to 0.35 $W \cdot m^{-1} \cdot K^{-1}$ of PA6/crushed-GF composites due to the destruction of GF. The TC of PB8GF composites reduced as high as 52% from 0.89 $W \cdot m^{-1} \cdot K^{-1}$ to 0.43 $W \cdot m^{-1} \cdot K^{-1}$ of PA6/crushed-B8GF composites. The greater reduction was caused by the 3D BNNSs thermal conductive path was destroyed in PA6/crushed-B8GF composites. The results reveal that both graphene and BNNSs formed a thermal conductive path in the PBGF composites. To further investigate the morphology of the 3D network in PBGF composites, the PBGF composites were washed by formic acid (see details in supporting information) to remove the free PA6 chains. BGF was regained (marked as regained BGF) with the original shape and size after washed. The SEM image in Fig. 8b also showed that the 3D framework was completely preserved and graphene sheets were covered with PA6 chains. This confirmed that polymer chains did be grafted onto graphene sheets. The favorable grafting enhanced the interfacial interaction between the graphene sheets and the PA6 matrix.

Another possible positive factor for the TC of PBGF composites is that BNNSs could patch up the defects of graphene sheets. Heat flow in BGF was shown in Fig. 7. Heat flows more freely where BNNSs filled the gap on graphene sheets. BGF and PBGF composites were subjected to EDS analysis to validate BNNSs were assembled in BGF. The EDS pattern of BGF and PBGF composites in Fig. 8c and

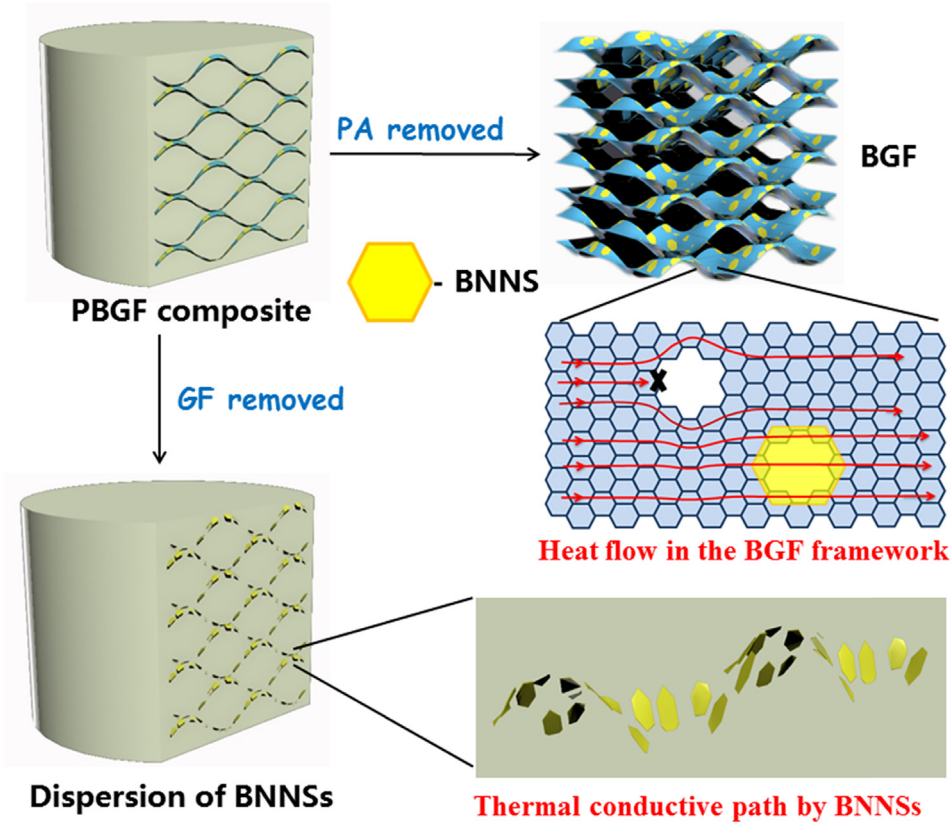

Fig. 7. Simulation schematic of the thermal conductive path in PBGF composites.

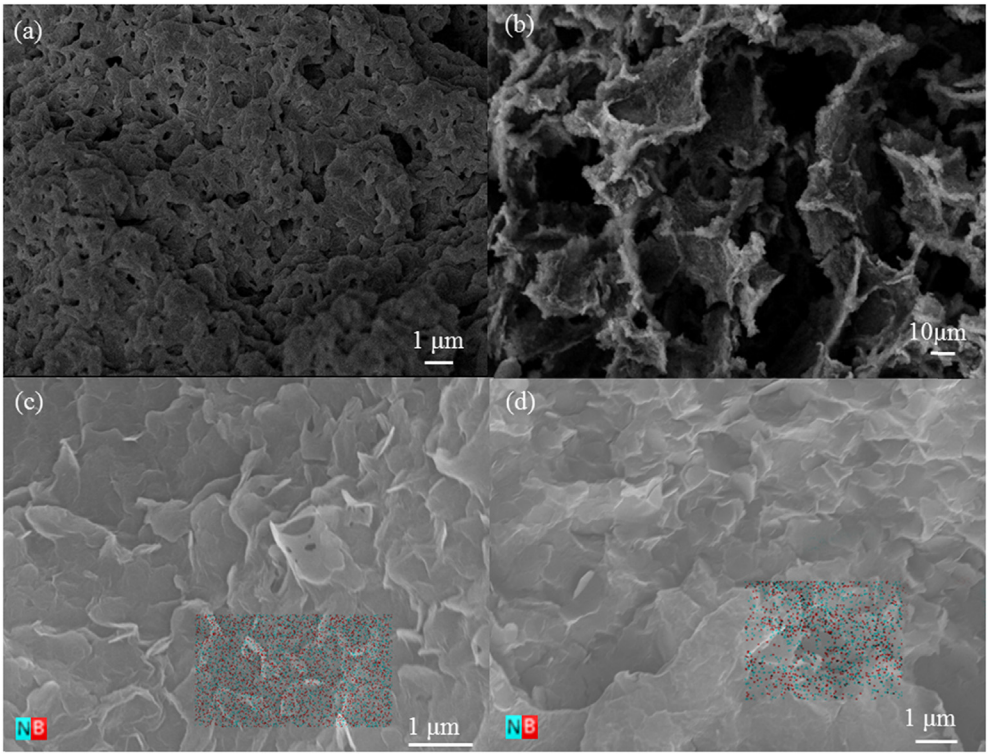

Fig. 8. SEM image of PA6/crushed-BGF composites (a) and regained BGF (b). EDS pattern of BGF (c) and PBGF composites (d).

d showed that B and N atoms were well-dispersed throughout BGF and PBGF composites. It shows that BNNSs were well-dispersed in BGF and maintained in PBGF composites by embedding onto graphene sheets. To further investigate the interaction between BNNSs and graphene sheets, the graphene hydrogel was used to absorb BNNSs. Graphene hydrogel and BNNSs were sealed in a 100 mL Teflon autoclave and maintained at 160 °C for 7 h. After the absorbing test, the solution was turbid (Fig. S5) and BNNSs cannot be physical absorbed by graphene hydrogel in a 160 °C sealed environment. This indicated that the embedded BNNSs in BGFs were not physically absorbed by graphene hydrogel. The bonding mechanism of BNNSs and graphene sheets might be the condensation reaction between functional groups generated in the solution exfoliation on BNNSs [45,46] and oxygenous groups on the GO sheets, as shown in Fig. S6. Moreover, the interaction between BNNSs and graphene sheets may be in favour of the phonon coupling of BGF. It was put forward that graphene sheets are very sensitive to their substrates and neighboring materials [47]. The rippling effect of graphene sheets may be suppressed by BNNSs was discussed in previous work [48–50]. It was confirmed by the experimental result that the change of the vibration mode of the 3D network caused to raise transfer efficiency of phonon [47,50].

4. Conclusion

In the present work, we prepared a hybrid 3D framework as thermal conductive filler in polymeric composites. We demonstrated the synergistic effect of BNNSs and graphene in the thermal conductive. An additional introduction of 1.6 wt% BNNSs could increase the TC up to 87.6% and 350% higher comparing with the composites containing 6.8 wt% graphene and neat PA6. The synergistic originated from the 3D hybrid framework: (1) BNNSs arranged to be a 3D thermal conductive path by using the 3D GF as a template; (2) BNNSs could patch up the defects of graphene sheets. The strategy of grafting PA6 chains to 3D hybrid framework made the layer filler dispersed uniformly without surface modification and improved the compatibility between filler and matrix. Finally, The TC of PA6 composite was improved efficiently due to the synergistic effect between BNNSs and graphene. Our work provides a new insight into the fabrication of composites with high performance for versatile applications in electronic device, high-temperature dielectric and energy store.

Conflict of interest

The authors declare no competing financial interest.

Acknowledgement

Prof. P. Ding acknowledges the financially support from the National Natural Science Foundation of China (51303101) and the funds for Scientific and Technological Innovation of Baoshan District in Shanghai (bkw2015136). The authors thank Prof. Yuliang Chu for help with the SEM measurements.

Appendix A. Supplementary data

Supplementary data related to this article can be found at http://dx.doi.org/10.1016/j.compscitech.2016.09.013.

References

[1] Q. Li, L. Chen, M.R. Gadinski, S. Zhang, G. Zhang, H. Li, et al., Flexible high-temperature dielectric materials from polymer nanocomposites, Nature 523 (7562) (2015) 576–579.
[2] J.F. Li, W. Lu, Y.B. Zeng, Z.P. Luo, Simultaneous enhancement of latent heat and thermal conductivity of docosane-based phase change material in the presence of spongy graphene, Sol. Energy Mater. Sol. Cells 128 (2014) 48–51.
[3] X. Fu, C. Yao, G. Yang, Recent advances in graphene/polyamide 6 composites: a review, RSC Adv. 5 (76) (2015) 61688–61702.

[4] G.-H. Kim, D. Lee, A. Shanker, L. Shao, M.S. Kwon, D. Gidley, et al., High thermal conductivity in amorphous polymer blends by engineered interchain interactions, Nat. Mater 14 (3) (2015) 295–300.
[5] Z.H. Cui, Z. Cao, R. Ma, A.V. Dobrynin, D.H. Adamson, Boron nitride surface activity as route to composite dielectric films, ACS Appl. Mater. Interfaces 7 (31) (2015) 16913–16916.
[6] H.-B. Cho, Y. Tokoi, S. Tanaka, H. Suematsu, T. Suzuki, W. Jiang, et al., Modification of BN nanosheets and their thermal conducting properties in nanocomposite film with polysiloxane according to the orientation of BN, Compos. Sci. Technol. 71 (8) (2011) 1046–1052.
[7] P. Ding, S. Su, N. Song, S. Tang, Y. Liu, L. Shi, Highly thermal conductive composites with polyamide-6 covalently-grafted graphene by an in situ polymerization and thermal reduction process, Carbon 66 (1) (2014) 576–584.
[8] S. Diaham, F. Saysouk, M.L. Locatelli, B. Belkerk, Y. Scudeller, R. Chiriac, et al., Thermal conductivity of polyimide/boron nitride nanocomposite films, J. Appl. Polym. Sci. 132 (34) (2015) 9.
[9] X. Wu, H. Liu, Z.H. Tang, B.C. Guo, Scalable fabrication of thermally conductive elastomer/boron nitride nanosheets composites by slurry compounding, Compos. Sci. Technol. 123 (2016) 179–186.
[10] B.X. Du, M. Xiao, Effects of thermally conducting particles on resistance to tracking failure of polyimide/BN composites, Ieee Trans. Dielectr. Electr. Insul. 21 (4) (2014) 1565–1572.
[11] Y. Hwang, M. Kim, J. Kim, Fabrication of surface-treated SiC/epoxy composites through a wetting method for enhanced thermal and mechanical properties, Chem. Eng. J. 246 (2014) 229–237.
[12] R.J. Warzoha, A.S. Fleischer, Effect of graphene layer thickness and mechanical compliance on interfacial heat flow and thermal conduction in solid-liquid phase change materials, ACS Appl. Mater. Interfaces 6 (15) (2014) 12868–12876.
[13] L.-C. Tang, Y.-J. Wan, D. Yan, Y.-B. Pei, L. Zhao, Y.-B. Li, et al., The effect of graphene dispersion on the mechanical properties of graphene/epoxy composites, Carbon 60 (2013) 16–27.
[14] H. Shen, J. Guo, H. Wang, N. Zhao, J. Xu, Bioinspired modification of h-BN for high thermal conductive composite films with aligned structure, ACS Appl. Mater. Interfaces 7 (10) (2015) 5701–5708.
[15] K.M. Nam, W. Kwon, S.-R. Kim, Y.K. Kim, et al., Biomimetic preparation of boron nitride/pmma composite, J. Korean Ceram. Soc. 51 (2) (2014) 103–106.
[16] H.L. Lee, O.H. Kwon, S.M. Ha, B.G. Kim, Y.S. Kim, J.C. Won, et al., Thermal conductivity improvement of surface-enhanced polyetherimide (PEI) composites using polyimide-coated h-BN particles, Phys. Chem. Chem. Phys. 16 (37) (2014) 20041–20046.
[17] P. Li Jun, H. Qi Shu, F. Xie, Insulating and thermally conductive composite filled with boron nitride particles, Adv. Mater. Res. 391–392 (2011) 282–286.
[18] X.L. Cui, P. Ding, N. Zhuang, L.Y. Shi, N. Song, S.F. Tang, Thermal conductive and mechanical properties of polymeric composites based on solution-exfoliated boron nitride and graphene nanosheets: a morphology-promoted synergistic effect, ACS Appl. Mater. Interfaces 7 (34) (2015) 19068–19075.
[19] S. Kemaloglu, G. Ozkoc, A. Aytac, Thermally conductive boron nitride/SEBS/EVA ternary composites: processing and characterization, Polym. Compos. 31 (8) (2010) 1398–1408.
[20] X. Yanming, J. Xing, F. Ying, L. Jing, L. Jie, R. Chunrong, et al., Boron nitride quasi-nanoscale fibers: controlled synthesis and improvement on thermal properties of PHA polymer, Int. J. Polym. Mater. Polym. Biomat. 63 (15) (2014) 794–799.
[21] K. Kim, H. Ju, J. Kim, Vertical particle alignment of boron nitride and silicon carbide binary filler system for thermal conductivity enhancement, Compos. Sci. Technol. 123 (2016) 99–105.
[22] W. Yu, H.Q. Xie, L.Q. Yin, J.C. Zhao, L.G. Xia, L.F. Chen, Exceptionally high thermal conductivity of thermal grease: synergistic effects of graphene and alumina, Int. J. Therm. Sci. 91 (2015) 76–82.
[23] H.C. Chang, H.J. Tsai, W.Y. Lin, Y.C. Chu, W.K. Hsu, Hexagonal boron nitride coated carbon nanotubes: interlayer polarization improved field emission, ACS Appl. Mater. Interfaces 7 (26) (2015) 14456–14462.
[24] S. Vinod, C.S. Tiwary, P.A. da Silva Autreto, J. Taha-Tijerina, S. Ozden, A.C. Chipara, et al., Low-density three-dimensional foam using self-reinforced hybrid two-dimensional atomic layers, Nat. Commun. 5 (2014).
[25] Z.F. Wang, Z.J. Tang, Q. Xue, Y. Huang, Y. Huang, M.S. Zhu, et al., Fabrication of boron nitride nanosheets by exfoliation, Chem. Rec. 16 (3) (2016) 1204–1215.
[26] C.L. Bao, L. Song, W.Y. Xing, B.H. Yuan, C.A. Wilkie, J.L. Huang, et al., Preparation of graphene by pressurized oxidation and multiplex reduction and its polymer nanocomposites by masterbatch-based melt blending, J. Mater. Chem. 22 (13) (2012) 6088–6096.
[27] K. Kiho, K. Myeongjin, H. Yongseon, K. Jooheon, Chemically modified boron nitride-epoxy terminated dimethylsiloxane composite for improving the thermal conductivity, Ceram. Int. 40 (1) (2014) 2047–2056.
[28] Z.Q. Kuang, Y.L. Chen, Y.L. Lu, L. Liu, S. Hu, S.P. Wen, et al., Fabrication of highly oriented hexagonal boron nitride nanosheet/elastomer nanocomposites with high thermal conductivity, Small 11 (14) (2015) 1655–1659.
[29] M. Du, Y.Z. Wu, X.P. Hao, A facile chemical exfoliation method to obtain large size boron nitride nanosheets, Crystengcomm 15 (9) (2013) 1782–1786.
[30] W.F. Chen, S.R. Li, C.H. Chen, L.F. Yan, Self-assembly and embedding of nanoparticles by in situ reduced graphene for preparation of a 3D graphene/nanoparticle aerogel, Adv. Mater. 23 (47) (2011) 5679.
[31] J.F. Shen, Y.Z. Hu, M. Shi, X. Lu, C. Qin, C. Li, et al., Fast and facile preparation of graphene oxide and reduced graphene oxide nanoplatelets, Chem. Mater. 21 (15) (2009) 3514–3520.
[32] Z. Xiuju, L. Zhidan, L. Bo, T. Shaozao, Improved thermal conductivity of composite particles filled epoxy resin, Adv. Mater. Res. 217–218 (2011) 439–444.
[33] C. Yuan, B. Duan, L. Li, B. Xie, M.Y. Huang, X.B. Luo, Thermal conductivity of polymer-based composites with magnetic aligned hexagonal boron nitride platelets, ACS Appl. Mater. Interfaces 7 (23) (2015) 13000–13006.
[34] H.C. Wu, M.R. Kessler, Multifunctional cyanate ester nanocomposites reinforced by hexagonal boron nitride after noncovalent biomimetic functionalization, ACS Appl. Mater. Interfaces 7 (10) (2015) 5915–5926.
[35] W. Dai, J. Yu, Z. Liu, Y. Wang, Y. Song, J. Lyu, et al., Enhanced thermal conductivity and retained electrical insulation for polyimide composites with SiC nanowires grown on graphene hybrid fillers, Compos. Part A Appl. Sci. Manuf. 76 (2015) 73–81.
[36] Y. Wu, F. Li, J. Huyan, X. Zou, Y. Li, Low dielectric and high thermal conductivity epoxy nanocomposites filled with NH2-POSS/n-BN hybrid fillers, J. Appl. Polym. Sci. 132 (19) (2015).
[37] G.P. Chen, W.L. Zhai, Z.H. Wang, J.G. Yu, F.Q. Wang, Y.N. Zhao, et al., Fabrication and supercapacitive properties of hierarchical porous carbon from polyacrylonitrile, Mater. Res. Bull. 72 (2015) 204–210.
[38] Z. Fan, F. Gong, S.T. Nguyen, H.M. Duong, Advanced multifunctional graphene aerogel – poly (methyl methacrylate) composites: experiments and modeling, Carbon 81 (0) (2015) 396–404.
[39] X. Li, L. Shao, N. Song, L. Shi, P. Ding, Enhanced thermal-conductive and anti-dripping properties of polyamide composites by 3D graphene structures at low filler content, Compos. A Appl. Sci. Manuf. 88 (2016) 305–314.
[40] H. Jung, S. Yu, N.S. Bae, S.M. Cho, R.H. Kim, S.H. Cho, et al., High through-plane thermal conduction of graphene nanoflake filled polymer composites melt-processed in an l-shape kinked tube, ACS Appl. Mater. Interfaces 7 (28) (2015) 15256–15262.
[41] H.J. Park, T.A. Kim, R. Kim, J. Kim, M. Park, A new method to estimate thermal conductivity of polymer composite using characteristics of fillers, J. Appl. Polym. Sci. 129 (3) (2013) 965–972.
[42] F. Orlando, P. Lacovig, L. Omiciuolo, N.G. Apostol, R. Larciprete, A. Baraldi, et al., Epitaxial growth of a single-domain hexagonal boron nitride mono layer, ACS Nano 8 (12) (2014) 12063–12070.
[43] S.J. Kim, K. Choi, B. Lee, Y. Kim, B.H. Hong, Materials for flexible, stretchable electronics: graphene and 2D materials, in: D.R. Clarke (Ed.), Annual Review of Materials Research, vol. 45, Annual Reviews, 45 Palo Alto, 2015, pp. 63–84.
[44] H.B. Cho, T. Nakayama, H. Suematsu, T. Suzuki, W.H. Jiang, K. Niihara, et al., Insulating polymer nanocomposites with high-thermal-conduction routes via linear densely packed boron nitride nanosheets, Compos. Sci. Technol. 129 (2016) 205–213.
[45] O. Cretu, H.P. Komsa, O. Lehtinen, G. Algara-Siller, U. Kaiser, K. Suenaga, et al., Experimental observation of boron nitride chains, ACS Nano 8 (12) (2014) 11950–11957.
[46] K. Mimura, M. Masaki, Y. Nakamura, T. Nishimura, Improvement in thermal conductivity of composite material filled with BN filler, Trans. Inst. Electron. Inf. Commun. Eng. C (2012) 434–438. J95-C(11).
[47] C.R. Dean, A.F. Young, I. Meric, C. Lee, L. Wang, S. Sorgenfrei, et al., Boron nitride substrates for high-quality graphene electronics, Nat. Nanotechnol. 5 (10) (2010) 722–726.
[48] C.H. Lui, L. Liu, K.F. Mak, G.W. Flynn, T.F. Heinz, Ultraflat graphene, Nature 462 (7271) (2009) 339–341.
[49] M. Ishigami, J.H. Chen, W.G. Cullen, M.S. Fuhrer, E.D. Williams, Atomic structure of graphene on SiO_2, Nano Lett. 7 (6) (2007) 1643–1648.
[50] H. Liem, H.S. Choy, Superior thermal conductivity of polymer nanocomposites by using graphene and boron nitride as fillers, Solid State Communications 163 (2013) 41–45.